INTERNATIONAL JOURNAL FOR NUMERICAL METHODS IN FLUIDS
Int. J. Numer. Meth. Fluids 2010; **63**:564–583
Published online 19 June 2009 in Wiley InterScience (www.interscience.wiley.com). DOI: 10.1002/fld.2093

An alternate approach for modelling of transient vaporous cavitation

K. S. Sumam[1,*,†,‡], S. G. Thampi[2,§] and N. Sajikumar[1,§]

[1]*Department of Civil Engineering, Government Engineering College, Thrissur-680009, Kerala, India*
[2]*Department of Civil Engineering, National Institute of Technology, Calicut, Kerala, India*

SUMMARY

Simulation of cavitating flow has been a thrust area of research for long period due to its practical and economic importance. The major hurdle in developing a numerical model for such flows is the difficulty in representing the quick phase changes, in general, and the alternate change of flow from single phase to two phase and back, in particular. In this case, instability due to sharp variation of flow characteristics also restricts the development of numerical models. The present study demonstrates the use of a relatively simple formulation for the analysis of flow characteristics in a quasi-rigid pipeline under abrupt phase changes due to cavitation. A popular scheme—MacCormack scheme—was used for developing a numerical solution for this problem. It uses the conservative form of the governing equations, viz. conservation of mass and momentum, the transport equation and the constitutive relationship. The model can handle variable properties of the water–vapour mixture, which is highly compressible. A newly introduced pressure under-relaxation method overcomes the numerical instability due to sharp variation of flow characteristics during phase change. The model could predict the instant of occurrence of vapour pressure, duration of persistence of vapour pressure and the rise of pressure due to vapour collapse to satisfactory levels with published data and experimental results. Copyright © 2009 John Wiley & Sons, Ltd.

Received 23 October 2008; Revised 13 April 2009; Accepted 18 April 2009

KEY WORDS: transient cavitation; compressibility; variable wave speed; vapour collapse; pressure under relaxation

1. INTRODUCTION

During the last several decades, considerable effort has been made, both experimentally and theoretically, to model the process of transient cavitation. Cavitation is the nucleation, growth and

*Correspondence to: K. S. Sumam, Department of Civil Engineering, Government Engineering College, Thrissur-680009, Kerala, India.
†E-mail: sumamkottekatt@yahoo.com
‡Senior Lecturer.
§Assistant Professor.

Contract/grant sponsor: Kerala State Council for Science, Technology & Environment

collapse of bubbles in the liquid of closed conduit flow, when the working pressure of the flowing liquid drops down to its vapour pressure. The collapse of the generated vapour bubbles in pipeline systems leads to the occurrence of the pressure surges, which is higher than water hammer pressure. The pressure surge caused by collapse of vapour bubble is one of the major concerns from the viewpoint of engineering applications. When cavitation occurs, severe degradation is observed in the performance of flow measuring/controlling devices, which manifests in different ways such as flow rate fluctuation, load asymmetry, vibrations and noise. In many cases, the system itself undergoes irrecoverable damages.

The phenomenon of water hammer together with transient cavitation was described by many authors [1–4]. The cavitation and consequent phase changes are really very complex processes. Normally, these are described by hyperbolic partial differential equations, which are not amenable to analytical solution. Numerical simulation of cavitating flows poses unique challenges, in terms of both modelling and developing robust numerical techniques for solution [5].

Wylie [2] simulated the formation of vaporous and gaseous cavitation in a pipe by means of discrete free gas model. This model was applied by him for a sudden closure of valve in a frictionless pipe from a constant head reservoir and found that numerical oscillations occur due to the existence of multiple cavities in the pipeline. Bergant and Simpson [4] modified the discrete cavity model into an interface model, by incorporating the interaction among the water hammer regions, distributed vaporous cavitation regions, intermediate cavities and cavities at boundaries in the pipeline. Bergant and Simpson [6] used shock equations for describing the condensation process and they reported that the magnitude of simulated pressure pulse in the interaction model is lower than that in the discrete model for the valve closure problem described earlier in the paragraph.

The method of characteristics approach was utilized in [7] for modelling the two-phase flow following the vaporous cavitation. The mass transfer during cavitation was ignored by them. Xie *et al.* [8] used a two-dimensional model for predicting cavitation process by using one-fluid model (homogeneous mixture flow). These models [7, 8] could predict the pressure transients for vaporous cavitation conditions following sudden closure of a valve in a pipeline, but high-frequency pressure oscillation that will normally occur immediately after collapse of vapour was not observed in the computed results.

Cannizzaro and Pezzinga [9] examined the effect of gaseous cavitation on thermic exchange between the gas bubbles and the surrounding liquid by means of a 2D model. They used continuity equations for gas, continuity equation for mixture, energy and momentum equations for the solution. The two-dimensional model of constant temperature and mass was able to predict the experimental data only at the first set of oscillations. They found that incorporation of thermic exchange between the gas bubbles and the surrounding liquid into the model improved the performance of the model. Senocak and Shyy [10] developed a pressure-based method for modelling a turbulent cavitating flow computation by utilising the continuity equation, Reynold's averaged Navier–Stokes equation, a volume fraction transport equation and constitutive relationship. It has been applied for the simulation of flow over a hemispherical object.

A variety of models right from relatively simple to very sophisticated and complicated models have been used to analyse the cavitation processes. However, these models suffer from one or other drawbacks. Simple formulations suffer from lack of prediction capability, whereas the complex and complicated formulations suffer from computational difficulty such as long computation time. It is felt that a compromise between the two—i.e. lack of prediction ability vs complexity of the model—needs to be drawn. Hence, a model with less complexity and less computational time is

DOI: 10.1002/fld

very much desirable. In this context, the present study was undertaken. It demonstrates the use of relatively simple formulation, i.e. flow equations for the homogeneous water–vapour mixture in conservative form for the prediction of flow characteristics in a quasi-rigid pipe under abrupt phase changes due to cavitation. Numerical simulation of cavitating flow involves the determination of four dependent variables, viz. mixture density, velocity of flow, mass fraction of vapour and pressure, at all grid points of the computational domain. Since there are four unknowns, four independent equations are needed for a unique solution to the problem. Several combinations of the governing equations are being utilized by various investigators [1, 3, 5, 10]. Although numerous models for cavitating flow have been reported in literature, a formulation based on the continuity equation for the water–vapour mixture, momentum equation for the mixture, transport equation for the vapour phase incorporating vaporisation and condensation processes, state law and the constitutive relationship has not been tried yet for simulating cavitating flow. In order to reduce the complexity of the model to the minimum possible level, such a combination is used here.

2. MATHEMATICAL MODEL

The present analysis is based on the following assumptions:

1. Generated vapour bubbles are uniformly distributed, they are very small in size and are spherical in shape. This assumption is valid in short duration transient cavitation events when the vapour bubbles are small in size and do not join together to form large cavities.
2. The difference in pressure across a bubble due to surface tension can be neglected.
3. The generated vapour bubbles and liquid have the same velocity, indicating the absence of slip between the two. Hence it allows the assumption of homogeneous mixture.
4. Vapour bubbles follows a polytropic compression law with the polytropic constant 'n' in the range 1.2–1.3.
5. Flow is one dimensional.

In short, the working medium is considered as a homogeneous mixture of two fluids (during vaporization) with properties varying from point to point depending on the relative ratio of the two phases.

2.1. Governing equations

The conservative form of one-dimensional continuity equation for homogeneous water–vapour mixture in [11] is given by

$$\frac{\partial \rho}{\partial t} + \frac{\partial (\rho v)}{\partial x} = 0 \tag{1}$$

and corresponding momentum equation is given by

$$\frac{\partial \rho v}{\partial t} + \frac{\partial (p + \rho v|v|)}{\partial x} + \frac{f \rho v|v|}{2D} = 0 \tag{2}$$

in which ρ, p, v, are the density, pressure and velocity of the mixture at any point in the pipe, respectively, D is the internal diameter of the pipe, x is the pipeline distance in the flow direction,

DOI: 10.1002/fld

t is the time, and f is the Darcy's friction factor. The vapour mass fraction f_v is governed by the transport equation in [5] and is given by

$$\frac{\partial(\rho f_v)}{\partial t}+\frac{\partial(\rho \mathrm{v} f_v)}{\partial x}=R_e-R_c \tag{3}$$

The source terms R_e and R_c denote the vapour generation (evaporation) and vapour collapse (condensation) rates, and are functions of flow parameters in [5] and are given by

$$R_e=C_e\frac{\sqrt{k}}{\sigma}\rho_l\rho_v\left[\frac{2}{3}\frac{p_v-p}{\rho_l}\right]^{1/2}(1-f_v) \tag{4}$$

$$R_c=C_c\frac{\sqrt{k}}{\sigma}\rho_l\rho_l\left[\frac{2}{3}\frac{p_-p_v}{\rho_l}\right]^{1/2}f_v \tag{5}$$

k is the turbulent kinetic energy, which is given as $\sqrt{k}=0.1v$, where v is the mean flow velocity, ρ_l, ρ_v are the instantaneous liquid, and vapour density, σ is the surface tension, p_v is the vapour pressure, and C_e and C_c are empirical constants and their recommended values are 0.02 and 0.01, respectively [5].

The gas equation is utilized for determining the ρ_v, during cavitation [12]. Chung and Lin [13] also considered the behaviour of steam be same as that of an ideal gas. The constitutive relationship connects the pressure with the rest of dependent variables and are given as

$$\rho=\rho_l(1-\alpha_v)+\alpha_v\rho_v \tag{6}$$

$$\rho_v=\frac{p}{RT} \tag{7}$$

$$\rho_l=\rho_{lo}\mathrm{e}^{(p-p_o)/K_l}\quad\text{(see [14])} \tag{8}$$

in which R is the gas constant, T the absolute temperature, α_v the volumetric fraction of vapour, and ρ_{lo}, p_o, K_l are the density, pressure, and bulk modulus of elasticity of the liquid at standard conditions. The effective bulk modulus K_{mix} and water–vapour mixture wave velocity a_{mix} during cavitation are given by following equations (see [15]):

$$\frac{1}{K_{mix}}=\frac{1}{K_l}+\frac{\alpha_v}{np}+\frac{cD}{Ee} \tag{9}$$

$$a_{mix}=\sqrt{K_{mix}/\rho} \tag{10}$$

in which c is the pipe constraint, e is the pipe wall thickness, E is the Young's modulus of elasticity of material of the pipe and n is the polytropic exponent of the gas. The first, second and third term in Equation (9) represents the effect of compressibility/expansibility of the liquid, the vapour and pipe material on bulk modulus, respectively. The equation of state was used to compute the change in fluid properties during transient conditions. Crespo *et al.* [16] stated that polytropic law can be assumed for gases while using Rayleigh–Plesset equation for bubble dynamics (though it is questionable) as the value of polytropic exponent is not very relevant for cavitation region.

The polytropic expansion of vapour bubble is given by

$$p\alpha^n=p_o\alpha_o^n \tag{11}$$

where the subscript '$_o$' represents the values at initial conditions.

DOI: 10.1002/fld

As the pressure varies along the pipeline, the volumetric fraction of vapour will also get affected at all the grid points. This variation is accounted by using Equation (11) in the following form:

$$\alpha_i^{k+1} = \left(\frac{p_i^k}{p_i^{k+1}}\right)^{1/n} * \alpha_i^k \tag{12}$$

in which indices 'i' and 'k' represent the grid locations along the length and time axes, respectively.

2.2. *Initial and boundary conditions*

The initial pressure at each discretisation point i can be determined by deducting the steady state frictional resistance up to that point from the upstream reservoir head H_o. Transient flow is generated by means of valve closure at the downstream end of the pipeline ($x = L$, where L is the total pipe length). The pressure at the boundary p_i^{k+1} can be computed from the continuity equation. At the upstream end, i.e. at $x = 0$ and for all $t > 0$, the pressure remains constant and is equal to the upstream reservoir head H_o.

3. NUMERICAL COMPUTATION

The discretization in the x-direction is performed in such a manner that it results in a whole number of stretches. Explicit method of computation is used in this study (because of the reason discussed in the latter part of this paper), and hence the time step has to be varied to satisfy the Courant–Friedrichs–Lewy (CFL) stability criteria, i.e. Δt is taken as the minimum value obtained by Equation (13):

$$\Delta t^k = \min\left[\frac{\Delta x}{|v_i| + a_{mix_i}}\right] \tag{13}$$

where Δx and Δt represent the grid size along the x- and t-axes, respectively, i represents the computational node and a_{mix_i} is pressure wave velocity in water–vapour mixture. The Equations (1)– (3) are rewritten in matrix form as follows:

$$\frac{\partial U}{\partial t} + \frac{\partial F}{\partial x} = S \tag{14}$$

in which

$$U = \begin{pmatrix} \rho \\ \rho v \\ \rho f_v \end{pmatrix}, \quad F = \begin{pmatrix} \rho v \\ p + \rho v|v| \\ \rho v f_v \end{pmatrix}, \quad S = \begin{pmatrix} 0 \\ \dfrac{f\rho v|v|}{2D} \\ R_e - R_c \end{pmatrix}$$

In this equation, F and U are used for brevity to represent the variables that vary both spatially and temporally. The MacCormack numerical scheme is adopted for the solution of the equations (Equations (1)–(3)) along with the constitutive relationship (Equation (6)). Though there had been certain reservations in using this scheme due to its so-called numerical damping, the method has been still in use. Cannizaro and Pezzinga [9] used it for predicting transient gaseous cavitation.

DOI: 10.1002/fld

This scheme incorporates a pseudo-time step in the computation in terms of two steps known as predictor and corrector steps.

Initially, the spatial derivatives are replaced by forward finite differences, for the predictor part

$$\frac{\partial F}{\partial x}=\frac{F_{i+1}^{k}-F_{i}^{k}}{\Delta x} \quad \text{and} \quad \frac{\partial U}{\partial t}=\frac{U_{i}^{p}-U_{i}^{k}}{\Delta t} \tag{15}$$

and by backward differences for the corrector part.

$$\frac{\partial F}{\partial x}=\frac{F_{i}^{p}-F_{i-1}^{p}}{\Delta x} \quad \text{and} \quad \frac{\partial U}{\partial t}=\frac{U_{i}^{c}-U_{i}^{p}}{\Delta t} \tag{16}$$

Indices, '^{p}' and '^{c}' refer to the predictor and corrector steps. The use of forward and backward finite differences is alternated in the predictor and the corrector steps at each subsequent time step. The dependent variables at new time are found by averaging the corrector value of the variable and the value of the variable at present time step.

3.1. Computational procedure

The computational procedure starts with the solution of the mass conservation equation, which provides the value of the mixture density ρ at a pseudo-time step. Then, the values of v and f_v in the time step are determined using Equations (2) and (3). The fourth variable pressure is evaluated from the constitutive relationship, which incorporates variable fluid property approach by treating the medium as a homogeneous mixture of two fluids (Equation (6)). The constitutive relationship is rewritten in the following form:

$$\rho_l(1-\alpha_v)+\alpha_v\rho_v-\rho=0 \tag{17}$$

The equation is then expressed in terms of the pressure in the new time step by using Equations (7), (8) and (12). Thus, the Equation (17) is reduced to the form $f(p)=0$, a nonlinear equation in pressure p_i^{k+1}

$$f(p_i^{k+1})=\alpha_{v_i}^{k}*\left(\frac{p_i^{k}}{p_i^{k+1}}\right)^{1/n}\frac{p_i^{k+1}}{RT}+\left(1-\alpha_{v_i}^{k}*\left(\frac{p_i^{k}}{p_i^{k+1}}\right)^{1/n}\right)\rho_{l_o}e^{(p_i^{k+1}-p_o)/K_l}-\rho_i^{k+1}=0 \tag{18}$$

The function $f(p)$ is a differentiable function in p_i^{k+1} and hence the Newton–Raphson method [17] is used for the solution of p in the new time step as follows:

$$p_i^{q+1}=p_i^{q}-\frac{f(p_i^{q})}{f'(p_i^{q})} \tag{19}$$

in which q is the iteration level, $f(p_i^q)$ is the function value at qth iteration and $f(p_i^q)$ is the value of the derivative of the $f(p)$ at qth iteration. Vapour mass fraction is converted into volume fraction using mixture density and density of vapour as $\alpha_v=f_v\rho/\rho_v$ (see [5]). With the known values of all the fluid properties at the present time step, the mixture density at the next time step, and an approximate initial value of pressure for the next time step (taken as pressure in the present time step), an improved estimate of pressure is obtained using Equation (19). This process is continued till successive values converge within the desired limits of accuracy.

DOI: 10.1002/fld

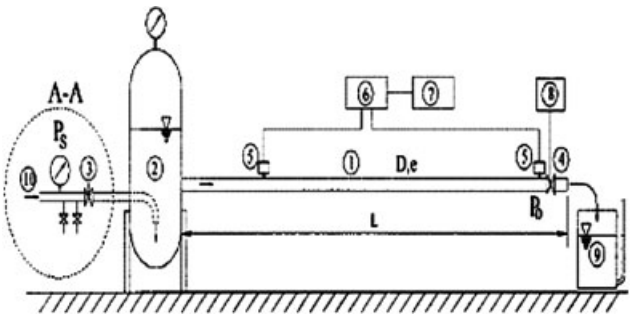

Figure 1. Schematic diagram of experimental set up (Experiment A [18]).

Table I. Physical properties of Experiment A and B.

Sl. no.	Material	Thickness (mm)	Diameter (mm)	U/s Pressure (0.1 MPa)	Discharge (m^3/s)	Name	Δx (m)	Time of closure (s)	T (°C)
1	Steel	3	41.9	2.03	0.0009	Experiment A [18]	0.5	0.021	8
2	Galvanised iron	3.7	52.76	1.67	0.00072	Experiment B	0.5	0.02	31–33

4. EXPERIMENTAL DATA

Experimental data from Mitosek [18] were used in this study to verify the efficacy of the described model. Unsteady flow was generated by the sudden closure of the valve mounted at the downstream end of the pipeline. A constant head was maintained at the upstream by means of the arrangement given in the Figure 1 and, hence, upstream boundary is taken as constant head reservoir. The valve closure time was measured with an accuracy of one in thousandth of a second. It ranged from 0.02 to 0.025 s in all the tests. The sampling time for recording pressure was chosen as 10^{-5} s. The steady-state velocity is 0.65 m/s. The tests were conducted at a constant temperature of 8°C. The details of the test set-up are given in Table I.

1, pipe; 2, reservoir; 3, pressure reducing valve; 4, ball valve; 5, strain gauge; 6, extensometer amplifier; 7, computer with AD/DA card; 8, valve closure time meter; 9, calibrated tank; 10, supply pipe.

5. RESULTS OF THE NUMERICAL MODEL

Though the procedure outlined in the previous section worked well in the water hammer pressure region, it became unstable as the computation approached the cavitation region, especially during vapour collapse. The instability appeared as negative absolute pressure in the iterative computation of pressure using Equation (19), which is not a physically realisable phenomenon. The possible reason for the occurrence of this is the linearization effect of the Newton–Raphson method, i.e. due to the exclusion of the higher-order terms in the derivation of Equation (19). In order to circumvent this difficulty, the computation of pressure was under-relaxed iteratively in a recursive manner so that the newly computed pressure of that iteration became positive, i.e. if the computed

DOI: 10.1002/fld

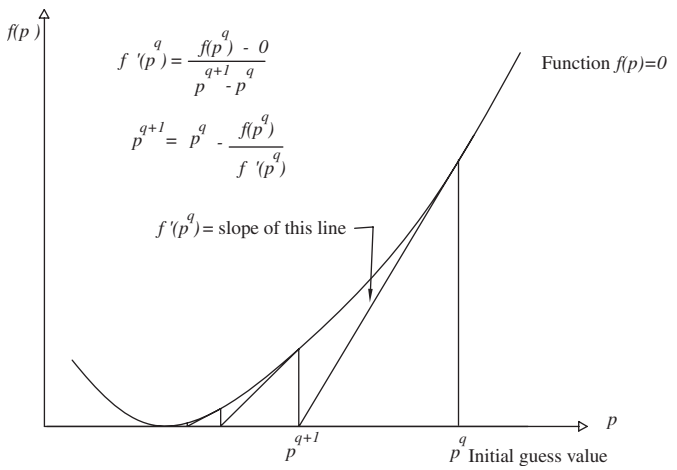

Figure 2. Solution procedure showing how the Newton–Raphson method approaches the root of an equation in normal situation.

pressure value in an iteration, became negative, the pressure correction term in Equation (19) (i.e. the second term) would be multiplied by a factor less than one (in the present study, its value is taken as 0.25). If computed pressure was still negative, the factor would be multiplied with itself so as to reduce the pressure correction factor further. This process was continued till the value of pressure in that iteration step became positive. It means that the trial solution moved along the tangent line to the original function till the pressure became positive. In order to have an insight into this process, two figures (Figures 2 and 3) are given. Figure 2 indicates how the solution procedure of Newton–Raphson method finds the root of an equation in normal situation. Figure 3 depicts a typical situation in which the Newton–Raphson method results in a physically unrealistic solution (negative root). It also indicates how an under-relaxation procedure overcomes this situation. Hence, under-relaxation procedure brings the pressure not only to the physically realisable range but also to the neighbourhood of final value of pressure in that iterative step, thereby reducing the number of iterations. The use of this under-relaxation procedure brought the model out of instability.

The model was run for one of the test cases from [18] for a steel pipe and the results are presented in Figure 4. While doing so the values of C_e and C_c in Equations (4) and (5) were taken as 0.02 and 0.01, as suggested in [5]. A close examination of generated volume of vapour indicated a gradual decrease in the volume fraction of vapour, which is not realistic in case of vapour collapse. Hence, a higher value of $C_c (C_c = 1)$ was selected so that sudden vapour reduction is obtained.

In Figure 4, the pressure first increases to a peak value, which is due to the water hammer effect, and then reduces to a very small value in the range of vapour pressure of the water. This low pressure persisted for some time till the next cycle of higher pressure returns. The persistence of pressure in the vapour pressure range generates vapour (as shown in the latter part of the paper). As the pressure increases during the next cycle, collapse of the generated vapour can occur, this in turn can result in very high pressure compared with water hammer pressure. But, in Figure 4, the collapse of vapour did not result in the expected high pressure, i.e. the maximum pressure after

DOI: 10.1002/fld

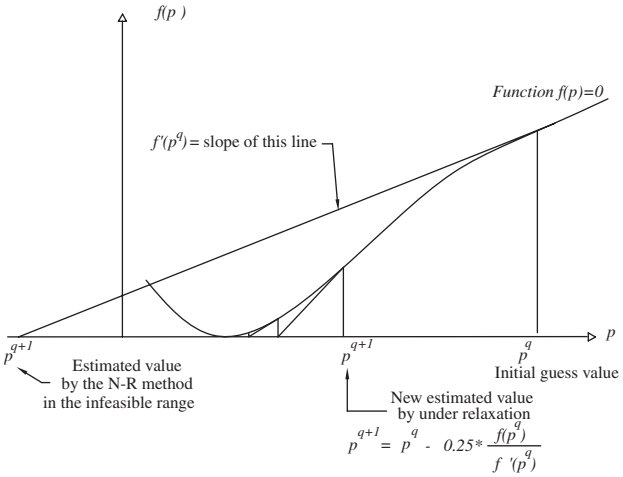

Figure 3. A typical situation where the Newton–Raphson method can lead to infeasible region of solution (negative value) and how under-relaxation procedure brings it back and then to solution.

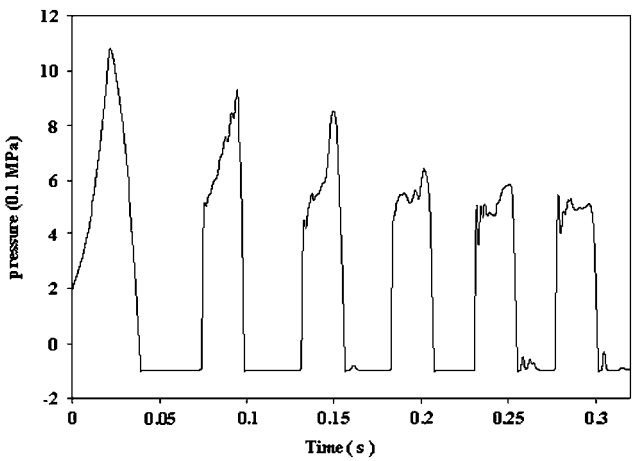

Figure 4. Computed pressure variation at exhaust valve, data from [18] ($v = 0.6\,\text{m/s}; t_c = 0.021\,\text{s}$).

the occurrence of vapour pressure (second peak in Figure 4) is less than the peak value of water hammer pressure (first peak in Figure 4). However, the pressure following the negative phase of water hammer showed continuous low-amplitude oscillations in the rising limb of the pressure curve. This is quite unnatural in the case of water hammer pressure wave. Also, no such oscillation was observed on the falling limb of the peaks. An examination of the corresponding experimental results reveals that there exists sharp pressure pulse of very high magnitude (compared with the water hammer pressure) and frequency in this region, possibly resulting from the collapse of vapour.

DOI: 10.1002/fld

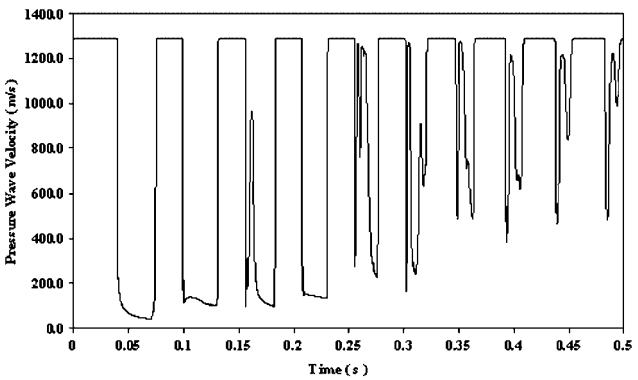

Figure 5. Computed wave velocity at exhaust valve data from [18] ($v = 0.6\,\text{m/s}$; $t_c = 0.021\,\text{s}$).

The computed wave velocity (Figure 5) also shows some indications of the sudden collapse of vapour. The wave velocity varies drastically from an order of thousands to a few metres/second in a very short period of time. This variation naturally indicates large variation in the bulk density of the fluid, which can happen only due to the generation of vapour/liberation of gases and their collapse. The drastic variation of wave velocity and low-amplitude oscillations in the rising limb of the pressure peak indicated collapse of generated vapour, but pressure peaks associated with the collapse were absent. What could be the possible reason for this mismatch?

Indication available in [18] helps us to throw light into this mismatch. It was reported that the sampling time could greatly influence the peak value shown by the data acquisition system (DAS). By conducting three tests with sampling times ($10^{-5}, 10^{-4}, 10^{-3}\,\text{s}$) it was found that high sharp peaks (spikes) were not noticed by the pressure transducers when sampling time has $10^{-3}\,\text{s}$; the transducer with sampling time $= 10^{-4}\,\text{s}$ could record some more peaks; the transducer with sampling time $= 10^{-5}\,\text{s}$ could indicate the sharp peaks as spikes. Can't this be the reason for the absence of peaks in computation even though the characteristics showed the collapse of vapour bubbles?

The wave velocity in the normal condition is about 1280 m/s, which results in a Δt value around 0.0004 s. However, during the cavitation process, the wave velocity reduces to 50 m/s or even less, which results in a Δt value of about 0.01 s. Coutier-Delgosha *et al.* [12] reported that the collapse of vapour could be so sudden that the particles of fluid may turn from vapour to pure liquid and back during the period of just one time step. Hence, it can be reasonably concluded that the absence of higher pressure peaks in the computed pressure variation curve was due to the inability of the time step to capture pressure pulses within it, as a result of using the time step Δt obtained based on the Courant stability criteria. Based on the above observations, a two thousands fold smaller Δt was used in this region for further computation, which in turn brought Δt to a value of $10^{-5}\,\text{s}$ or even less.

Computations were carried out for the same data by reducing Δt as mentioned above to an order of $10^{-5}\,\text{s}$ or even less. The modified Δt did not remain constant as the original Δt was calculated from CFL criteria. The results are shown in Figure 6. It could be seen from this figure that several pressure peaks with magnitude larger than water hammer pressure appear in the results immediately after the vapour collapse, justifying the argument presented in the previous paragraphs. However, there is a difference in the oscillating behaviour of the computed and experimental pressure curve

DOI: 10.1002/fld

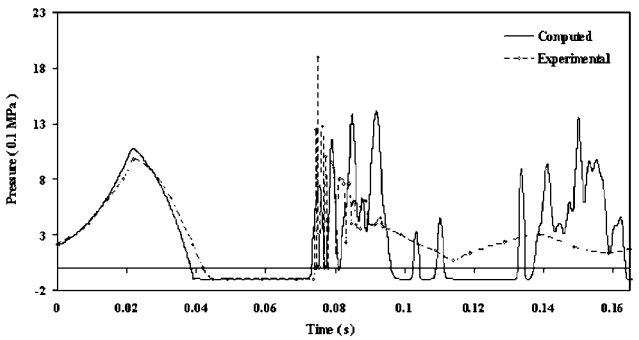

Figure 6. Pressure comparison at exhaust valve by using many folds smaller Δt [18], ($v = 0.6\,\mathrm{m/s}$; $t_c = 0.021\,\mathrm{s}$).

(Figure 6). In the experimental curve, the pressure moves up to a maximum value suddenly and then it oscillates and comes down to the negative part of the pressure wave. But, in computation, the pressure oscillates and moves up to the maximum value and oscillates and comes down to the negative part of the pressure wave. This difference in behaviour may be due to the very sharp slope of pressure variation curve (sometimes amounting to near discontinuity).

It can also be seen that the computed and experimental pressure curves match very well with respect to the water hammer pressure, the starting time of vapour collapse and the duration for which vapour pressure persists. The model was able to compute the pressure peaks due to vapour collapse, which is higher than the water hammer pressure. However, the predicted value is less than the maximum peak pressure reported in the experiment (1.4 MPa against 1.9 MPa). The water hammer pressure wave is matching well with the pressure wave, obtained from the experiment. Thereafter the pressure remains in the vapour pressure region as indicated by the straight line region, i.e. the pressure remains around 2540 Pa and thus generated vapour (given by R_e in Equation (4)). It can be seen that the model could match the peak values except for the sharp pressure spike. Moreover, there is a very small shift in the occurrence of this maximum pressure spike. However, the model could predict the magnitude of the second largest pressure peak of vapour collapse.

In order to make the argument fool proof, one has to answer the following question. Can these oscillations be due to the numerical error owing to the use of very small Δt than that obtained from CFL criteria? The wave velocity in the normal condition is 1280 m/s, whereas in cavitation, it is 25 m/s. The corresponding Δt from CFL criteria (for $\Delta x = 0.5\,\mathrm{m}$) are 0.0004 and 0.02, respectively. While vapour collapses, sharp density change occurs, that too within a single time step. Here, the model has to compute pressure hikes with $\Delta t = 0.02\,\mathrm{s}$. But the Δt calculated by CFL for the next time step $t + \Delta t$ is 0.0004 s, i.e. when such a sharp change in velocity occurs within a time step as indicated by Coutier-Delgosha *et al.* [12], should it be more reasonable to use a smaller Δt corresponding to next time step than it at the present time so that the variation of phenomenon is well represented in the time domain. CFL criteria are normally used based on the assumption that wave velocity do not vary drastically from one time step to other. If it occurs otherwise, should it be more reasonable to refine the Δt so that the variation of phenomenon is well represented.

It is also interesting to note that there are no oscillations available in the negative phase of pressure (with sharp negative gradient) and also in computation. If the oscillation due to numerical error were present it would have appeared in both the cases where sharp density gradient exists. Hence, this qualitative assessment of results reveals that the numerical error is limited.

DOI: 10.1002/fld

For predicting pressure spikes due to vapour collapse, a very small Δt (approximately, 2000 times smaller than the Δt obtained using Courant stability criteria) is required to be used. This situation does not favour the use of an implicit method. The advantage of using an implicit method is that it permits the use of a large Δt, due to the absence of any restriction in Δt such as CFL criteria, since implicit methods are unconditionally stable. Hence, the use of implicit method is not recommended in this case.

Further, the examination of Figure 6 indicates that the pressure due to vapour collapse damps very strongly, indicating that cavitation oscillations are damped very easily. This is well in agreement with the observations in [18]. However, there is a distinct behaviour shown by the model, i.e. water hammer pressure cycles are not damped so fast as we have noticed in the experimental results. The pressure in the experiment is damped easily to the normal working pressure within a few cycles of oscillation (within 0.16 s) while in computation it oscillates for a longer period. The possible reasons for this are (i) the extra damping effects due to some fittings in the experimental set-up; and (ii) inability of the model to simulate the damping effect. It is necessary to identify the exact reason (from the above two) for the discrepancy mentioned in this paragraph.

In order to have an insight into this behaviour, the model was run for another experimental data from [18], in which the pressure diagrams at two locations, viz. at the valve and at a location 12 m upstream of the valve were reported. In order to see how the water hammer peaks get damped, the pressure curve at the valve (Figure 7(a)) was used as the boundary condition and the pressure at a location 12 m upstream of the valve was predicted. The computed vs experimental pressure curves are given in Figure 7(b). The computed peak lies above the experimental peak. It is reasonable to infer that the high pressure due to cavitation at the downstream end could affect the pressure variation 12 m upstream. This can produce high pressure at 12 m, as noticed in the computation, if there is no artificial damping effect. A damping from 2.8 to 0.7 MPa (75% damping) could not be expected, as the distance between the points of measurement is only 12 m. (The damping reported by Chaudhry *et al.* [19] for similar experimental set-up, between two sections separated at a distance of 9.5 m, is only about 20%.) The computed values of pressure are in good agreement with the experimental values except for the peak value corresponding to the collapse of vapour at the valve. All these observations point towards artificial damping which may be due to the arrangement provided on the upstream of experimental set-up to maintain a constant head. Direct verification of this observation is not possible as the data are taken from the literature. Hence, an experimental study was conducted to verify the performance of the model.

The experimental study was carried out on an installation in the Water Flow Laboratory of the Fluid Control Research Institute, Palakkad, Kerala, India. The schematic diagram of the set up and relevant details are given in Figure 8. A galvanized iron pipe of length L ($L=34.15$ m), internal diameter $D=52.76$ mm and a pipe wall thickness $=3.7$ mm was used for conducting the experimental investigation. The friction factor f was evaluated by conducting experiments at steady state and was found to be 0.03. The pipe was fed with a constant discharge from a constant head tank (CHT). The temperature of the water was maintained between 31 and 33°C. Unsteady flow conditions were created by the sudden closure of a quick acting butterfly valve (QAV) mounted at the end of the pipe. The valve closure time was measured and was found to be in the range of 0.02–0.021 s in all the tests. This is less than or equal to the wave period of pressure oscillations. A PCI-MIO-16E1 data acquisition system (DAS) with sampling capacity of 1.25 million samples/second was used. However, a sampling rate of 1 lakh samples per second was adopted in the study, the sampling time being 10^{-5} s.

DOI: 10.1002/fld

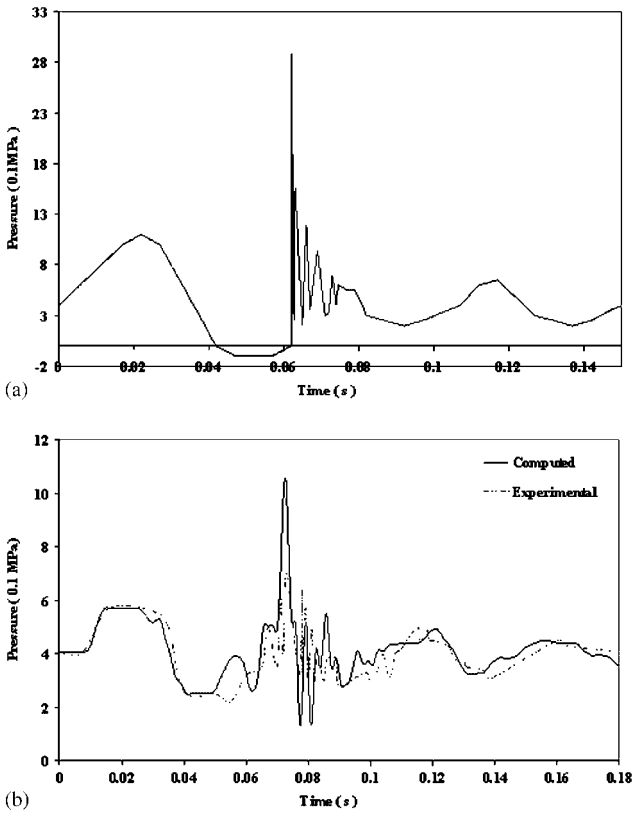

Figure 7. (a) Pressure curve at exhaust valve as boundary condition [18], ($v_o = 0.6\,\mathrm{m/s}$; $t_c = 0.022\,\mathrm{s}$) and (b) pressure curves at 12 m, upstream of exhaust valve.

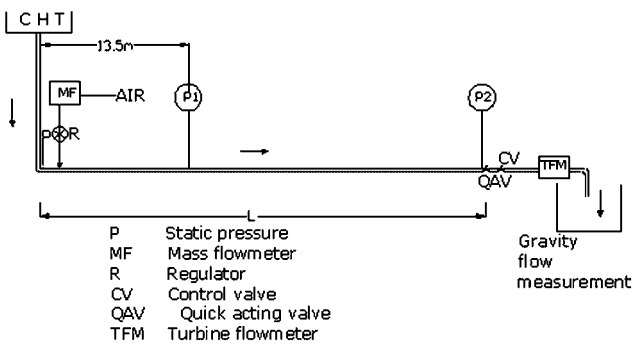

Figure 8. Schematic diagram of experimental set-up (B).

The experiment was conducted for a flow rate $0.000746\,\mathrm{m^3/s}$, which corresponds to a steady-state velocity of 0.34 m/s. The pressure variation curve due to sudden closure of quick acting valve was measured (Figure 9). In this paper, hereafter the experiment from [18] will be referred to as

DOI: 10.1002/fld

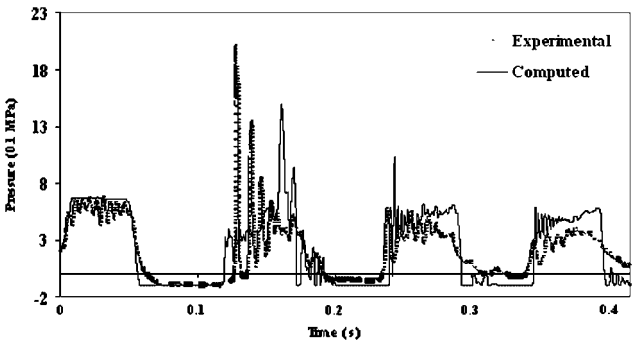

Figure 9. Pressure Curves at QAV (Experiment B).

the experiment A and the experiment conducted at FCRI as experiment B. The physical properties and numerical set-up are given in Table I.

It can be seen from Figure 9 that the pressure goes below atmospheric pressure for peaks after vapour collapse, if not to vapour pressure, in the negative phase of the pressure wave. This reduction of pressure to vapour/negative pressure does not happen in experiment A (Figure 6). It is also interesting to note that the flow velocity in experiment B is about half the flow velocity in Experiment A. A higher velocity should always lead to a lower value of pressure in the negative phase of the water hammer wave, other conditions remaining the same. In addition, the length of the pipeline used in experiment B is more than the length used in experiment A. Smaller the length of the pipeline, the lesser should be the damping effect. Owing to these reasons (small velocity and larger length) the pressure curve of experiment (B) should show more damping effect when compared to that of [18]. But, a review of the experimental results (Figures 6 and 9) reveals that damping effect is less in the experiment B compared with experiment A, i.e. though conditions are favourable for the occurrence of negative/vapour pressure for subsequent wave cycles in experiment A, no negative pressure is seen to occur in this case. All these, points towards the effect of artificial damping on peaks subsequent to the peak due to vapour collapse in the experiment in [18] and emphasizes the observations reported earlier in this section regarding the artificial damping effect. However, this does not affect the initial phase of cavitation and the magnitude of pressure hikes immediately after vapour collapse, as this absorbance (damping), if present, will occur only after arrival of the negative phase of the water hammer pressure wave to the chamber in the experimental set-up reported in [18].

As observed in the computations carried out using data from experiment A, the pressure following vapour collapse oscillates up to the peak, and then oscillates down to the negative phase of the pressure wave (Figure 9). Reasons for such a behaviour have been indicated earlier in the discussion on the results of experiment A. The oscillating behaviour appears in both experiments A and B and hence the model behaviour is consistent. The model could predict the pressure due to vapour collapse, though the predicted maximum pressure is slightly less than the experimental peak (1.5 MPa against 2.0 MPa). This is also consistent with the results discussed earlier (experiment A). Besides, the subsequent crest and trough of the pressure curve also matche with the experimental results (Experiment B). This behaviour is inconsistent with the results discussed earlier and emphasizes that the artificial damping effect in experiment A is due to absorbance by the fittings. Hence, the discrepancy (extra damping) observed in the results from the mathematical

DOI: 10.1002/fld

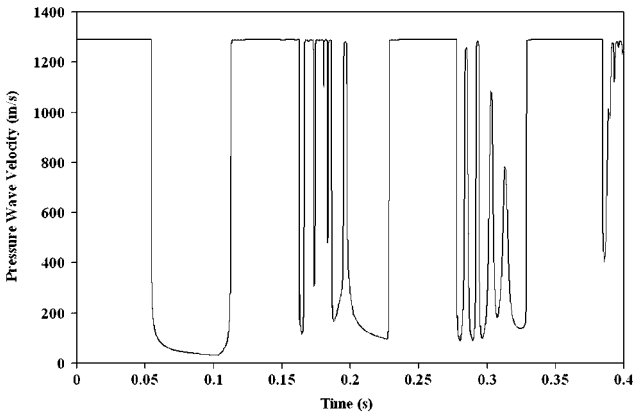

Figure 10. Computed wave velocity (Experiment B).

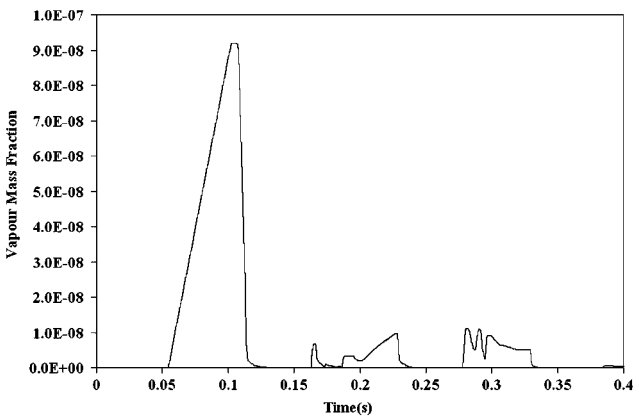

Figure 11. Generated vapour mass fraction (Experiment B).

model with reference to the results of experiment A is not due to the weakness of the model but due to the experimental set up itself.

To have an insight into the behaviour of the developed model, the computed wave velocity and generated vapour mass fraction corresponding to Experiment B are plotted in Figures 10 and 11. The wave velocity goes down to a few metres per second, justifying the line of thought presented in the earlier part of the paper. The corresponding generated vapour (in terms of mass fraction) also shows a steady increase till the end of the vapour pressure region and then collapses. The vapour collapse is indicated both by the drastic increase in wave velocity and sudden decrease in vapour mass fraction. It is interesting to note that the fluctuations in the wave velocity have corresponding variation in the generated vapour volume. These also reinforce the fact that the model could not only predict the characteristics of pressure variation but also that of wave velocity and generated vapour.

DOI: 10.1002/fld

Table II. Experimental runs for model validation.

Run no.	Upstream pressure (0.1 MPa)	Length (m)	Discharge (m^3/s)	Figure numbers	Identification	Time of closure (s)
1	1.67	32.5	0.000562	Figure 12	Experiment C	0.02
2	1.67	32.5	0.00072	Figure 13	Experiment D	0.02
3	1.67	32.5	0.00075	Figure 14	Experiment E	0.02

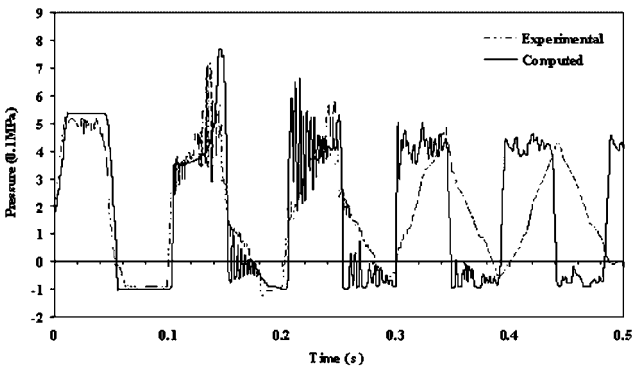

Figure 12. Pressure curve at QAV, (C) ($H_o = 1.67\,\text{MPa}$, $Q_o = 0.000562\,\text{m}^3/\text{s}$, $t_c = 0.02\,\text{s}$).

In order to confirm that the model performed satisfactorily, three more experimental runs were carried out. These data were used for verifying model performance. Details of these experiments are given in Table II. In all the simulations carried out with the mathematical model, the valve closure characteristics were taken as the downstream boundary condition.

Results of simulations carried out with these experimental data show that the model exhibits the same trend and behaviour as described earlier, i.e. the water hammer pressure forms an envelope over the experimental water hammer pressure peak and then it drops to the vapour pressure region. These results are presented in Figures 12–14. The pressure wave velocity is very small in vaporous cavitation region and the pressure (both experimental and computational) remains at the vapour pressure until its increase is forced by the main water hammer wave. The vapour present in the pipeline collapses at this stage, resulting in sharp pressure hikes, which again causes cavitation. But its intensity decreases with time. At low flow rates, the cavitation duration exactly coincides with that observed in the experiment for the first two pressure peaks after the collapse of vapour (Figures 12–14). It is interesting to note that the deviation of computed pressure curve from the experimental curve increases with discharge. Moreover, it is observed that if the vapour fraction reaches an order of 10^{-7}, the vapour collapses with a spike of pressure peak and in that case the computed peak value is less than the experimental value (Figure 14 for case E). On the other hand, if the vapour fraction is much less than this value, no such single spike is observed.

Though the general trend of the computed and measured pressure curves match well, there exists a difference in the amplitude of pressure wave from the 4th wave cycle. It is seen that the difference gets progressively amplified the pressure wave moves over many cycles. Such as behaviour has also been observed in [20, 21]. The study of Bergant and Simpson [22], in which

DOI: 10.1002/fld

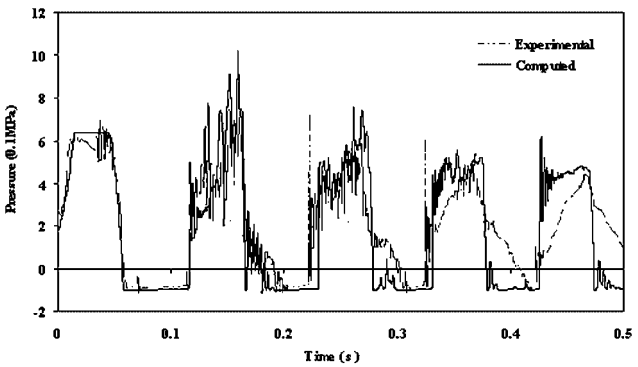

Figure 13. Pressure curve at QAV, (D) ($H_o = 1.67\,\text{MPa}$, $Q_o = 0.00072\,\text{m}^3/\text{s}$, $t_c = 0.02\,\text{s}$).

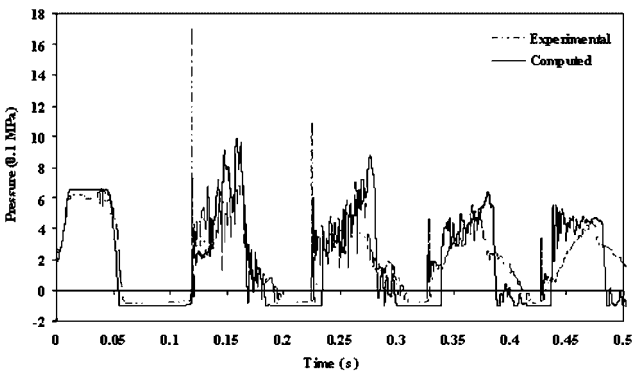

Figure 14. Pressure curve at QAV, (E) ($H_o = 1.67\,\text{MPa}$, $Q_o = 0.00075\,\text{m}^3/\text{s}$, $t_c = 0.02\,\text{s}$).

they compared the effect of steady friction vs unsteady friction in the prediction of transient cavitation, throws some light on this difference. It was observed that the use of a steady friction formula could result in a difference between the computed pressure wave and the measured one in subsequent peaks after the cavitation pressure peak. The difference increases progressively as the pressure wave passes through many cycles. However, it was found that this difference diminishes if the effect of unsteady friction is incorporated into the model. The effect of unsteady friction is more predominant in transient turbulent flows with low Reynolds number. The difference between the amplitude of the computed and the measured pressure waves in the present situation can be explained in terms of the unsteady friction, which is not accounted for in the developed cavitation model. Moreover, when the pressure goes below the vapour pressure (which is always less than the saturation pressure of dissolved gas), the liberation of dissolved gas can occur. The release of gas is not accounted in the present model, which in turn can also contribute to the difference in behaviour of the model mentioned at the earlier part of the paragraph. These reasons individually or jointly can contribute to the deviation between computed and measured pressure variation curve.

However, Bergant and Simpson [22] pointed out that the first pressure pulse does not differ irrespective of whether unsteady friction is incorporated into the model or not. Also, this does not

DOI: 10.1002/fld

affect the cavitation pressure peaks and its oscillation. Since the basic aim of the present study is to develop and demonstrate the performance of a mathematical model for predicting the rise of pressure due to vapour collapse which is not affected by unsteady friction (see [22]), no attempt has been made to incorporate the effect of unsteady friction into the present model.

In short, the developed relatively simple model can predict the cavitation and effect of vapour collapse to a satisfactory level, though not to exemplary levels. This fact should be viewed in context of the level of complexity used in the model.

6. CONCLUSIONS

The following conclusions can be drawn from this study.

(i) A numerical model is developed for the prediction of transient cavitation with relatively simple governing equations.
(ii) In order to overcome the instability associated with drastic changes in flow characteristics due to abrupt phase changes, pressure under relaxation can be effectively used.
(iii) The suggested procedure for modelling evaporation/condensation in [5] can effectively represent the processes, provided the empirical constants in the transport equation are properly adjusted.
(iv) Prediction of pressure due to cavitation requires Δt much smaller than that specified by the Courant—stability criteria so that it matches with the next time step. Hence, the use of implicit method has limited advantages.
(v) The model could predict the time of occurrence of vapour pressure, duration of its persistence, instant of vapour collapse and the maximum rise of pressure due to vapour collapse to satisfactory levels.
(vi) The difference in amplitude of computed and measured pressure wave for the fag end of the pressure transient can be explained in terms of the unsteady friction and gas release, which is not accounted in the present model.

NOTATION

The following symbols are used in this paper:

A	pipe cross-sectional area
a_{mix}	pressure wave velocity in water–vapour mixture
c	parameter for pipe constraint
^{c}	notation for corrector method
C_c	constant in vapour condensation
C_e	constant in evaporation
D	pipeline mean diameter
e	local pipe-wall thickness
E	Young's modulus of elasticity
f	Darcy–Weisbach friction factor
f_v	vapour mass fraction
g	acceleration due to gravity

DOI: 10.1002/fld

H_o	reservoir head
i	subscript for grid loction along x (space direction) axis, $L = i\Delta x$
K_{mix}	effective bulk modulus of water-vapour mixture
K_l	bulk modulus of the liquid
k	turbulence kinetic energy
k	time level at $t = \sum \Delta t^k$, turbulent kinetic energy
L	length of the pipe
l	subscript for liquid (water)
N	number of node points
n	polytropic compression index, 1.2–1.3 ; Iteration number
o	subscript for the initial state conditions
p	absolute pressure
p	notation for predictor method
p_o	Standard pressure
p_v	water vapour pressure
Q_o	Initial flow rate
q	iteration number
R	gas constant
R_e	rate of Evaporation
R_c	rate of Condensation
t	instantaneous time in transient flow
t_c	time of closure of the valve
T	absolute temperature
v	flow velocity
x	pipeline distance
z	pipeline elevation

Greek alphabets

α_o	initial volume fraction of gas
α_v	volumetric fraction of vapour
ρ	water–vapour density
ρ_l	water (Liquid) density
ρ_v	vapour density
ρ_{l_o}	water (Liquid) density at standard conditions
σ	surface tension
Δx	node point distance along pipeline
Δt	increment in time
Δt^k	time-step at kth time level

ACKNOWLEDGEMENTS

The authors acknowledge the financial assistance by the Kerala State Council for Science, Technology & Environment (KSCSTE, as per council order no (T)123/SRS/2005/CSTE Dated Thiruvananthapuram, 29.03.05), Kerala, India. The writers also acknowledge the Fluid Control Research Institute, India, for providing all necessary facilities to conduct the experiment in their Water Flow Laboratory.

DOI: 10.1002/fld

REFERENCES

1. Kranenburg C. Gas release during transient cavitation in pipes. *Journal of Hydraulic Division* (ASCE) 1974; **100**(9):1383–1398.
2. Wylie EB. Simulation of vaporous and gaseous cavitation. *Journal of Fluids Engineering* (ASCE) 1984; **106**: 307–311.
3. Simpson AR, Wylie EB. Large water hammer pressures for column separation in pipelines. *Journal of Hydraulic Engineering* 1991; **117**:1310–1315.
4. Bergant A, Simpson AR. Interface model for transient cavitating flow in pipelines. In *Unsteady Flow and Fluid Transients*, Bettess, W (eds). The Netherlands: Balkema, Rotterdam, 1992; 333–342.
5. Singhal AK, Athavale MM, Li H, Jiang Y. Mathematical basis and validation of full cavitation model. *Journal of Fluids Engineering* (ASCE) 2002; **124**:617–624.
6. Bergant A, Simpson AR. Pipeline column separation flow regimes. *Journal of hydraulic engineering* (ASCE) 1999; **125**(8):835–848.
7. Shu J. Modelling vaporous cavitation on fluid transients. *International Journal of Pressure Vessels and Piping* 2003; **80**:187–195.
8. Xie WF, Liu TG, Khoo BC. Application of a one fluid model for large scale homogeneous unsteady cavitation: The modified Schmidt model. *Computers and Fluids* 2006; **35**(10):1177–1192.
9. Cannizzaro D, Pezzinga G. Energy dissipation in transient gaseous cavitation. *Journal of Hydraulic Engineering ASCE* 2005; **131**(8):724–732.
10. Senocak I, Shyy W. A pressure-based method for turbulent cavitating flow computations. *Journal of Computational Physics* 2002; **176**:363–383.
11. Falk K, Gudmundsson JS. Waterhammer in high pressure multiphase flow. *Pressure Surges* 2000; @BHR Group, 2000: 41–54.
12. Coutier-Delgosha O, Fortes-Patella R, Reboud JL, Hakimi N, Hirsch C. Stability of preconditioned Navier Stokes equations associated with a cavitation model. *Computers and Fluid* 2005; **34**:319–349.
13. Chung NM, Lin WK. Sound velocity and its relationship with interfacial area density in a steam/water, two-phase bubbly flow. *Flow Measurement and Instrumentation* 1992; **3**(2):65–71.
14. Hadj-Taieb E, Lili T. Validation of hyperbolic model for water hammer in deformable pipes. *Journal of Fluids Engineering* (ASME) 2000; **122**(1):57–64.
15. Lee TS, Ngoh KL. Air entrainment effects on the pressure transient of pumping systems with weir discharge chamber. *Journal of Fluids Engineering* (ASME) 2002; **124**:1034–1043.
16. Crespo A, Garcia J, Fernandez JJ. Stability criteria of the steady flow of a liquid containing bubbles along a nozzle. *Journal of Fluids Engineering* (ASME) 2001; **123**:836–840.
17. Press WH, Teukolsky SA, Vetterling WT, Flannery BP. *Numerical Recipes in C*. Cambridge University Press: 1992.
18. Mitosek M. Study of transient vapour cavitation in series pipe systems. *Journal of Hydraulic Engineering* 2000; **126**(11):904–911.
19. Chaudhry MH, Bhallamudi SM, Martin CS, Naghash M. Analysis of transient pressures in bubbly homogeneous gas-liquid mixtures. *Journal of Fluids Engineering* (ASME) 1990; **112**:225–231.
20. Silva-Araya WF, Chaudhry MH. Computation of energy dissipation in transient flow. *Journal of Hydraulic Engineering* 1997; **123**(2):106–115.
21. Pezzinga G. Evaluation of unsteady flow resistances by quasi-2D or 1D models. *Journal of Hydraulic Engineering* (ASCE) 2000; **126**(9):778–785.
22. Bergant A, Simpson AR. Estimating unsteady friction in transient cavitating pipe flow. *Second International Conference on Water Pipeline System*. BHR group Ltd: Edinburgh, Scotland, U.K., 24–26 May 1994; 3–16.

DOI: 10.1002/fld